Optics & Laser Technology 145 (2022) 107477

Contents lists available at ScienceDirect

Optics and Laser Technology

journal homepage: www.elsevier.com/locate/optlastec

Multi-beam single-photon LiDAR with hybrid multiplexing in wavelength and time

Di Wu [a], Tianxiang Zheng [a], Linli Wang [a], Xiuliang Chen [a], Lei Yang [a], Zhaohui Li [a], Guang Wu [a,b,*]

[a] State Key Laboratory of Precision Spectroscopy, East China Normal University, Shanghai 200241, China
[b] Collaborative Innovation Center of Extreme Optics, Shanxi University, Taiyuan 030006, China

ARTICLE INFO

Keywords:
Multi-beam
3D imaging
Single-photon LiDAR

ABSTRACT

We report a multi-beam single-photon light detection and ranging (LiDAR) in eye-safe band at 1.5 μm with hybrid multiplexing in wavelength and time. 16 independent laser diodes with equal frequency spacing in dense wavelength division multiplexing (DWDM) were combined with a blazed grating to generate multi-beam dispersing with equal angle in space as the LiDAR laser source. Meanwhile, time division multiplexing (TDM) was applied on the 16 laser diodes as well. A single-pixel single-photon detector (SP-SPD) was used to detect the echo photon signal of all laser beams by TDM. In this way, we constituted a compact optical system without multi-beam transceiver alignment. The LiDAR system was simple and robust with this hybrid multiplexing technology. An outdoor photon-counting imaging within 75-m range was achieved, with the laser power lower than 1/10 of the human eye safety threshold. It has high application potential in the field of automatic driving with strict eye safety requirements.

1. Introduction

In recent years, LiDAR has been developing rapidly in the fields of laser mapping [1–2], industrial measurement [3–6], and automatic driving [7–8]. Multi-beam LiDAR can effectively improve the measurement field of view and speed, which makes Velodyne's LiDARs widely used in the field of automatic driving [9]. However, due to the limitation of total laser power, the energy of single laser beam decreases linearly with the increase of the beam number, which greatly reduces the ranging distance of multi-beam LiDAR. Single-photon LiDAR (SPL) improves the detection sensitivity to sparse photons by using single-photon detector and is suitable for long-distance or low-power applications [10–16], which makes the SPL have great advantages in multi-beam LiDAR. The Leica SPL100 splits a 532 nm laser into 10 × 10 laser beams and receives the echo photons by a 10 × 10 single-photon detection array of photomultiplier tube (PMT). It reached to 6 million points per second with a 60 kHz pulse repetition rate, which was the fastest LiDAR as far as we known [17]. In 2017, we realized a multi-beam SPL [18]. A 532-nm laser split into 1 × 100 beams through a diffractive optical element, and their echo photons were collected into a 1 × 100 fiber array and detected by 100 silicon avalanche photodiode single-photon detectors one-on-one. Both SPLs required precise multi-beam transceiver alignment, which was not conducive to mass production. In order to simplify the system, frequency multiplexing photon-counting method was proposed [19]. Sixteen beams of individually triggered laser diodes output through fiber array, and their echo photons detected by a single-pixel single-photon detector (SP-SPD). Recently, a wavelength-time coding method has been applied to single-photon detection. A pulsed supercontinuum laser source conjunction with an acousto-optic tunable filter (AOTF) were used to output discrete pulse trains of different central frequencies and delay. This method improved the spectral response and depth resolution by simultaneously detecting the echoes of the multiple-wavelength lasers with a SP-SPD [20]. In addition, a time-stretch LiDAR modulated broadband light source by spectro-temporal encoded to generate multi-wavelength light beam with controllable time delay [21]. Then, the multi-wavelength laser was diffracted into multi beams, and their echo photons were also detected by a SP-SPD. In this way, the scanning range and measuring distance of the SPL were greatly extended. These LiDARs developed multiplexing technologies to simplify the detection. However, in order to realize the long-distance and multi-beam measurement, these wavelength-time coding method usually need the extra time delay modulation device,

* Corresponding author at: State Key Laboratory of Precision Spectroscopy, East China Normal University, Shanghai 200241, China
E-mail addresses: zhhli@lps.ecnu.edu.cn (Z. Li), gwu@phy.ecnu.edu.cn (G. Wu).

https://doi.org/10.1016/j.optlastec.2021.107477
Received 4 May 2021; Received in revised form 26 July 2021; Accepted 23 August 2021
Available online 27 August 2021
0030-3992/© 2021 Elsevier Ltd. All rights reserved.

which will increase the complexity of the SPL.

In this paper, we designed a simple and robust SPL system with hybrid multiplexing technique in wavelength and time. 16 independent laser diodes with equal frequency spacing in DWDM were combined with a blazed grating to generate multi-beam dispersing with equal angle in space as the LiDAR laser source. Meanwhile, TDM was applied on the 16 laser diodes as well. A field programmable gate array (FPGA) board was used to freely adjust the time delay between different wavelength laser diodes to realize flexible adjustment of the measurement distance. The optical path of single-beam transceiver and multi-beam detection was constructed based on a blazed grating and a multi-wavelength laser source. The 16-beam scanning imaging was realized in the field of view of 45° × 20° within the range of 75 m outdoor. In addition, the main components of the SPL come from the fiber communication industry, which is mature, reliable, and cheap, and is conducive to large-scale production.

2. The SPL with wavelength and time multiplexing

2.1. The coaxial transceiver

Fig. 1 is the schematic diagram of the multi-beam coaxial transceiver. A multi-wavelength laser source with fiber pigtail was achromatically collimated in space. Then, the laser beam passed through a perforated mirror, and was incidents on a blazed grating. The diffractions of the multi-wavelength laser propagated to different direction according to

$$\alpha[sin(\theta_i) + sin(\theta_m)] = m\lambda \quad (1)$$

where $\theta_i$is the angle between the incident light and the normal line on the grating surface, θ_m is the output angle as measured from the surface normal of the blazed grating, λ is the laser wavelength, m is the order of principal maxima, and α is the groove spacing. On the other hand, the echo photons were also diffracted by the blazed grating in the same way and return to the perforated mirror. According to Eq. (1), the diffracted light of echo light could be coaxial with the outgoing laser beam. Then the light was reflected to a focusing lens and coupled into a multimode fiber to the SP-SPD for detection. The dispersion of the blazed grating was 0.62 mrad/nm, while $\theta_i = 45^\circ$. For the light of each wavelength from 1500 nm to 1600 nm, the fiber and blazed grating determine its receiving field angle of 0.45 mrad. The wavelength spacing between adjacent lasers was about 1.6 nm, resulting in the angle between adjacent beams of ~ 1.0 mrad. Totally, the receiving angle of the blazed grating was set to ~ 15 mrad through a conical baffle, corresponding to the receiving spectral bandwidth of ~ 25 nm.

2.2. The multi-wavelength laser and the time-division-multiplexing SP-SPD

In the time-stretch LiDAR, the multi-wavelength laser was distilled from a broadband laser source by spectro-temporal modulation. However, the broadband laser is expensive and not robust for the application of LiDAR. Moreover, it cannot distill narrow linewidth light, e.g., ~2 nm at 1550 nm, which is not conducive to compress the bandwidth of the filter, and the divergence angle of the output laser beam will be seriously broadened by the grating dispersion. Meanwhile, the multi-channel optical fiber delay is complex and cannot be adjusted flexibly according to different measurement range.

We developed a multi-wavelength laser source with narrow linewidth. 16 distributed feedback (DFB) lasers (Micro photons (Shanghai) Technology Co., Ltd.) were used, which was manufactured for DWDM fiber communication as shown in Fig. 2. The DFB lasers had a narrow linewidth as low as 3 MHz and had a broadband modulation bandwidth up to 2.5 GHz. The delay between laser pulses of each wavelength can be flexibly adjusted, as each laser diode was driven independently. As shown in Fig. 2, a FPGA board generated 17 pulse trains with the repetition rate of 100 kHz, one of which was the "start" for time-to-digital converter (TDC), and the other 16 channels were the laser trigger signals, with a delay of 500 ns in turn. Then, the DFB lasers were triggered to generate short pulses with the pulse duration of ~ 0.5 ns. They were in C-band ITU grid wavelengths, and the central frequencies were from 191.8 THz to 194.8 THz with equal frequency spacing of 200 GHz. The 16 lasers were combined with a dense wavelength division multiplexer and amplified by an erbium doped fiber amplifier (EDFA). The spectrum of the output light from the EDFA was measured as shown in Fig. 3. The laser spectrum was similar to the frequency comb with the spacing of 200 GHz. In the spectrum, each "comb tooth" was generated by an independent DFB laser, but in time regime there was time delay of 500 ns between adjacent beams. There was no stable carrier phase relationship between different channels, which does not matter for LiDAR application. According to Eq. (1), the diffraction angle between adjacent beams was nearly 1.0 mrad, when the laser beam was incident on the blazed grating at 45°.

The average power of each laser beam was 0.4 mW to 0.8 mW with the repetition of 100 kHz after the EDFA. The laser energy was 4 nJ to 8 nJ per pulse with the laser pule width of 0.5 ns. The total output power of all 16 laser was 9.6 mW. The multi-beam SPL was eye safety, as the eye safety threshold was 10 mW according to the IEC 60,825 standard of the International Electrotechnical Commission. Moreover, the laser beams would gradually separate with the propagation, as the angel between the adjacent laser beams was 1 mrad. When the propagation exceeds 8 m, two laser beams would not incident on a same eye at the same time. At this moment, only the effect of a single laser beam on the eyes needs to be considered, which was 10 times lower than the human

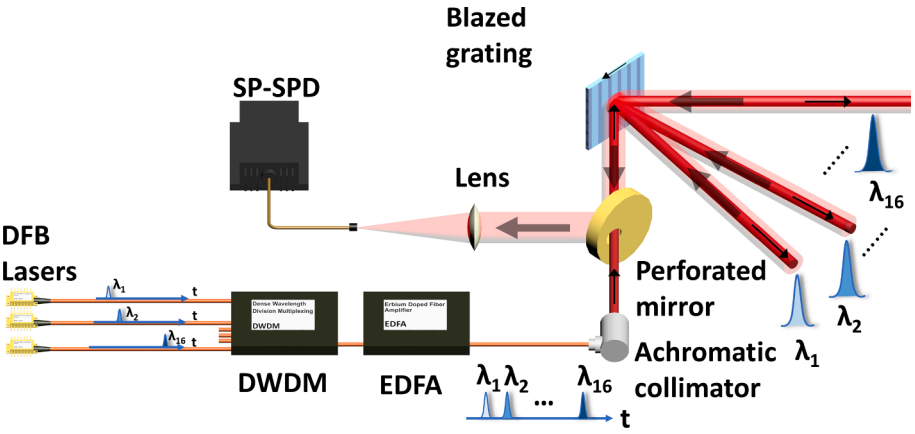

Fig. 1. The schematic diagram of the multi-beam coaxial transceiver. Achromatic collimator: output beam size is 12 mm in diameter, full angle beam divergence is 0.02° (Thorlabs RC12APC-P01). Blazed grating: the size is 50 × 50 × 9.5 mm, groove is 600/mm, blazed wavelength is 1600 nm, θ_m = 194.11 mrad @ 1500 nm and θ_m = 255.67 mrad @ 1600 nm while θ_i = 45°, (Thorlabs GR50-0616). Focusing lens: D = 30.0 mm, F = 100.0 mm. Reflector: D = 50 mm, the diameter of the hole is 12 mm. Multimode fiber: fiber core is 62.5 μm in diameter.

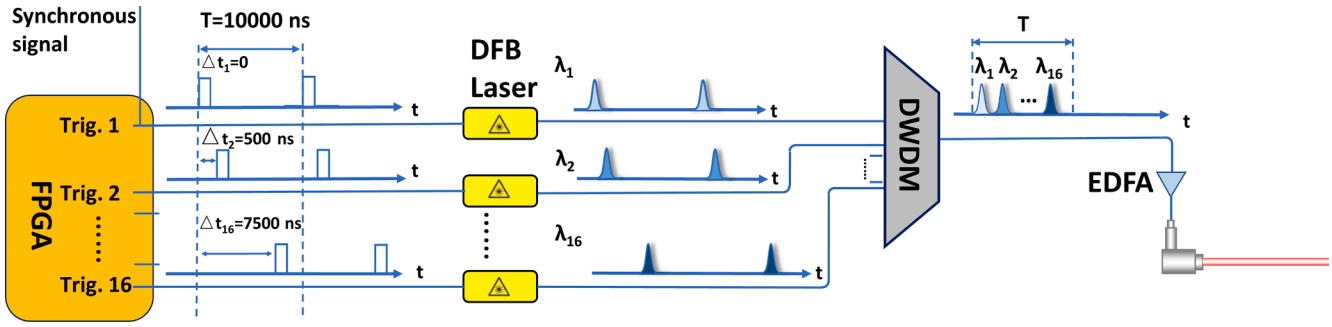

Fig. 2. The generation principle of the multi-wavelength laser. DFB lasers: A laser whose output wavelength varies with the working temperature. DWDM: Dense wavelength division multiplexer. EDFA: Erbium doped fiber amplifier. T is the period of the pulses.

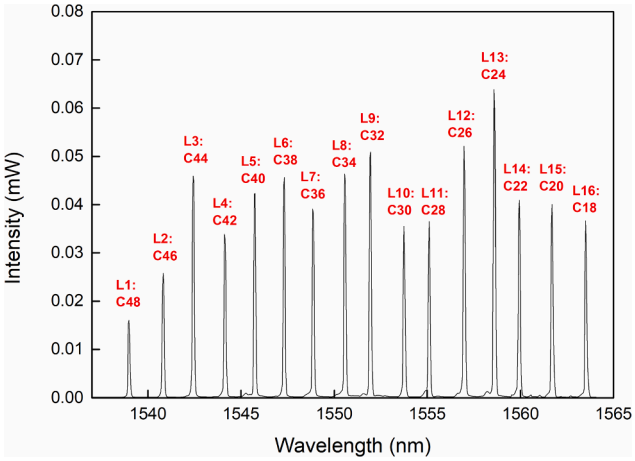

Fig. 3. The spectrum of the multi-wavelength laser. According to the wavelength from short to long, we numbered each DFB from Laser No. 1 (L1) to Laser No. 16 (L16).

eye safety threshold.

Fig. 3 is the spectrum of the multi-wavelength laser after being amplified by EDFA, which was detected by an optical spectrum analyzer (OSA) (AQ6370DOSAO, Yokogawa). The wavelength of each DFB laser was modulated by changing its working temperature, and monitored by the OSA. The temperature tuning coefficient of laser wavelength was 0.1 nm/°C, the resolution of OSA was 0.02 nm, and the linewidth of the lasers operated in pulsed mode was measured as 0.12 nm, which was limited by the precision of the OSA.

In the experiment, we used a SP-SPD to detect all the echo photons. The SP-SPD was a Geiger-mode InGaAs/InP avalanche photodiode. It was operated in 1.0-GHz sine wave gated mode to obtain short dead time [22], which was very useful to detect the signal photon under strong ambient illumination. The SP-SPD was used to detect all the echo photons without synchronization with the laser pulses, which was so-called quasi free-running mode [23].

As shown in the Fig. 4, in time-correlation single-photon counting (TCSPC) measurement, the obvious counting peaks of the echo photons from the targets would be formed with multiple periods of accumulation. The noise counts of the ambient light and dark counts of the SPD would be accumulated to background as they are randomly distributed in time. Although the noise counts may be larger than the signal counts in total, the signal peaks are much higher than the background. After filtering the noise by setting the threshold for the counts, the depth was extracted from the counting peaks by using the centroid method to calculate the TOF.

There was a time delay of 500 ns between the laser pulses of each wavelength in a single period. When the measured distance was limited to 75 m, the time-of-flight (TOF) signal of the echo photon of each laser was within 500 ns, and there was no crosstalk between the lasers of each wavelength. Therefore, the echo signals could be distinguished by TDM in the range of 75 m according to

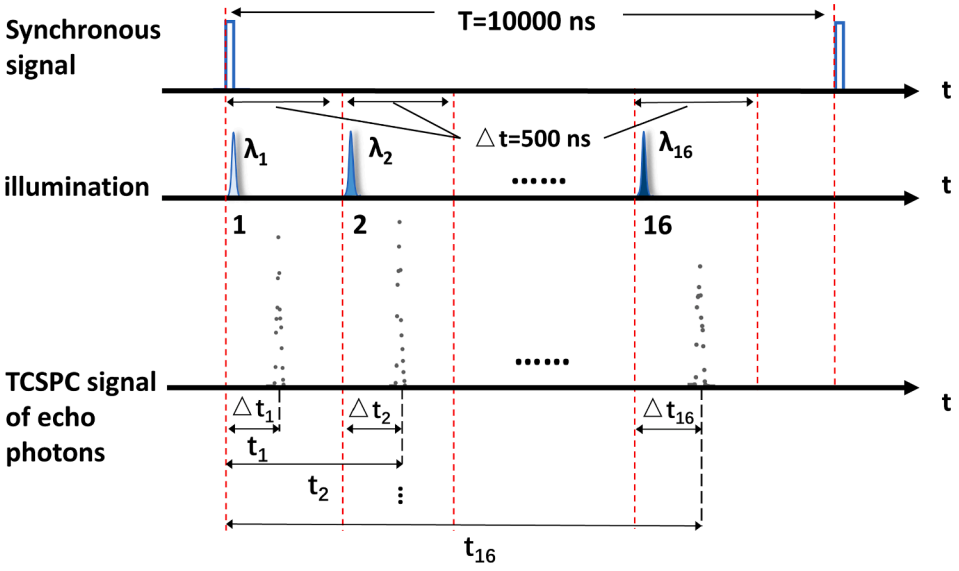

Fig. 4. The measurement principle of time division multiplexing.

$$\begin{aligned} n &= \lceil (t_n - t_{syn} - t_0)/500 \rceil, \\ \Delta t_n &= t_n - t_{syn} - t_0 - 500(n-1), \\ L_n &= c\Delta t_n/2. \end{aligned} \tag{2}$$

where t_n is the timing of the SP-SPD output, n is the laser beam number, t_{syn} is the timing of the synchronization signal, t_0 is the fixed delay of the detection (~266.2 ns), Δt_n is the TOF of the echo photon of the n^{th} laser beam, c is the speed of lights, L_n is the distance measured by the nt^h laser beam.

Fig. 5(a) is the TCSPC measurement of the outdoor test in the daytime. The detection efficiency of the SP-SPD used in this experiment was 0.5%, the dark count rate of the SP-SPD was 4.6×10^6 count per second (cps), the background noise was 8×10^5 cps, and the echo photon count rate of the all the laser beams from the cement floor 14-m away was 1.1×10^6 cps. According to the echo photon signal of L2, the temporal resolution of the SPL was approximately 0.8 ns, which was mainly determined by the time jitter of the SP-SPD and the pulse width of the laser. The wavelength of the multi-beam laser source used in this experiment ranged from 1538.98 nm to 1563.05 nm. According to the refractive index of near infrared in the atmosphere [24], the dispersion delay of this multi-wavelength laser was about 9.8×10^{-6} ns for the to-and-fro propagation of 75 m, which was far smaller than the time jitter of the detector and could be ignored.

In TCSPC measurement, the detection accuracy of the SPL was related to the photon counts. The relationship between the root mean square error (RMSE) and the accumulation time is shown in Fig. 5(b). As the accumulation time increases, the photon counts increases, and the RMSE of the measurement decreases. The average photon counts were $\sim 1 \times 10^6$ counts with the accumulation time of 1 s, while the RMSE of the measurement was about 11 ps, corresponding to the distance precision of 1.7 mm.

3. Results and discussions

The multi-beam SPL was installed on a two-dimensional rotating platform for scanning imaging. The rotating platform was set to 16 mrad/step in the horizontal direction, and 6 mrad/step in the vertical direction, as the 16 laser beams were distributed in the horizontal direction. The cumulative time of each step was 1 s. After rotating the platform 50 steps in the horizontal direction and 60 steps in the vertical direction, the surroundings within the range of 75 m × 20 m × 5 m was measured and formed a 3D cloud points of 800 × 60 pixels as shown in Fig. 6. The window depth was 14.0 cm, and the air conditioner height was 51.0 cm, which can be clearly shown in Fig. 6(b). We selected the data points of 50 m away from the wall in Fig. 6(d) and got the distance precision was 25 mm by linear fitting. The photon intensity was 3×10^4 counts, and the ranging precision was 2.2 mm according to Fig. 5(b). The main measurement error was induced by the rotators with the precision of ~ 0.02°. Three bicycles were used to simulate the scenes that might be encountered during the driving of the vehicle, which could be distinguished clearly in the point cloud image as shown in Fig. 6(c).

The measurement time of Fig. 6 was about 1 h, because the cumulative time was 1 s per point. Considering the application of real-time measurement, the cumulative time needs to be reduced. According to Fig. 5(b), the cumulative time can be greatly reduced at the cost of minor reduced measurement precision. The RMSE of the measurement was 262 ps, corresponding to the distance precision of 39.3 mm, when the cumulative time of measurement was shortened to 1 ms. Moreover, the echo rate showed two orders of magnitude improvement possibility, since the laser power was 10 times lower than the eye safety threshold, and the detection efficiency of the SP-SPD could be increased to greater than 5% by choosing high-performance Geiger-mode InGaAs/InP APD. Compared to the fiber-coupled SPD, the spatially-coupled SPD can collect more echo photons, which can also increase the performance of the multi-beam SPL. As a result, the cumulative time can be further reduced.

The number of beams is another important index of multi-beam SPL. The 50-GHz DWDM has more than 80 channels in C-band, which can support more than 80 eye-safe laser beams for the multi-beam SPL. In the experiment, the echo photons of 16 beams were detected by only one SP-SPD by using TDM technology. However, the number of beams will be limited by the saturation count rate of the SPD since all the photons from different channels were detected by the same SPD. And the repetition rate of the pulsed laser and the delay between the lasers should be increased to extend the maximum unambiguous range of 75 m. However, it will decrease the imaging speed. To solve these problems, the advantage of the multi-beam SPL could be used since the laser source employed DWDM technology. In the detection part, a demultiplexer can used to divide the echo beams into several channels according to the wavelength and be detected by different SPDs separately.

4. Summary

In conclusion, we demonstrated a multi-beam SPL with hybrid-multiplexing technique, which showed several striking features. Firstly, a blazed grating and a multi-wavelength laser source were used to form a single-beam transceiver and multi-beam detection optical structure, which was simple and robust. Secondly, the multi-beam SPL used 16C-band DWDM laser diodes with equal frequency spacing and time-sharing trigger, so that only one single-pixel single-photon detector could detect all the echo photons. And most of the devices came from the optical communication industry, which was convenient for large-scale production. Finally, after 8 m of laser transmission, the multi-beam

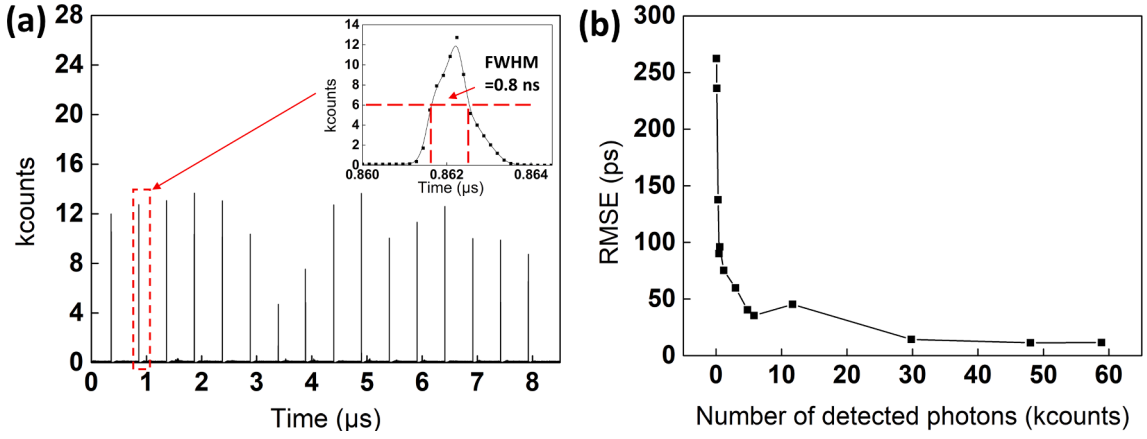

Fig. 5. (a) The echo photon signal of all lasers collected by TDC when the accumulation measurement time was 1 s. (b) The measurement accuracy of the SPL at different accumulation times.

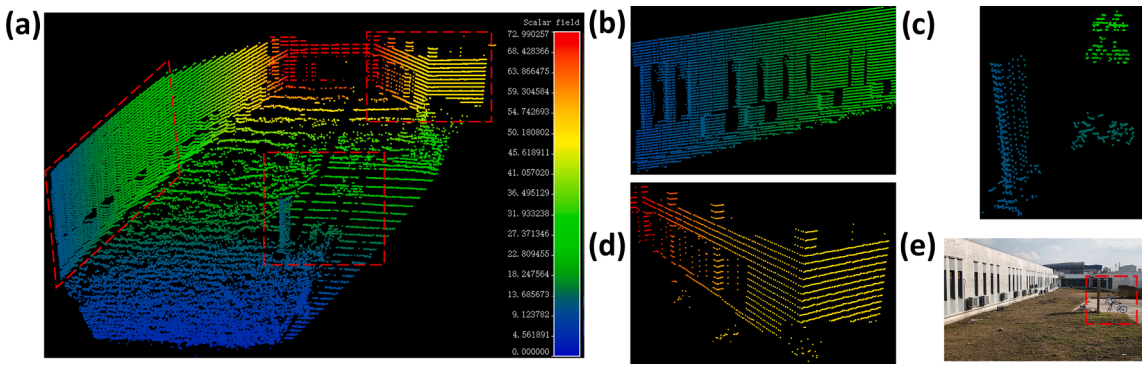

Fig. 6. (a) The reconstructed 3D image of the building and its surroundings. (b) Detail of the window image in the red dashed line box on the left in (a). (c) Detail of the road sign and bicycle image in the red dashed line box in the middle of (a). (d) Detail of the building corner image in the red dashed line box on the right in (a). (e) The photo of the building and its surroundings.

SPL was 10 times lower than the human eye safety threshold, which was very useful in the field of eye-safe laser ranging. A high-precision 3D imaging in the range of 75 m was realized with the precision of 1.7 mm. The multi-beam SPL has great space to improve the measurement speed and beam number and has great application potential in the field of automatic driving.

Funding

This work was supported by National Key Technologies R&D Program of China (2016YFB0400904); National Natural Science Foundation of China (11774095, 11804099, and 11621404); Shanghai Basic Research Project (No.18JC1412200).

CRediT authorship contribution statement

Di Wu: Conceptualization, Methodology, Software, Investigation, Formal analysis, Visualization, Writing – original draft, Writing – review & editing. **Tianxiang Zheng:** Investigation, Resources. **Linli Wang:** Methodology, Software, Resources. **Xiuliang Chen:** Investigation, Resources. **Lei Yang:** Software, Data curation. **Zhaohui Li:** Methodology, Investigation, Visualization. **Guang Wu:** Conceptualization, Methodology, Investigation, Writing – original draft, Resources, Writing – review & editing, Supervision, Project administration.

Declaration of Competing Interest

The authors declare that they have no known competing financial interests or personal relationships that could have appeared to influence the work reported in this paper.

References

[1] D.J. Lum, S.H. Knarr, J.C. Howell, Frequency-modulated continuous-wave LiDAR compressive depth-mapping, Opt. Exp. 26 (12) (2018) 15420–15435.
[2] M.R. Roddewig, J.H. Churnside, F.R. Hauer, J. Williams, P.E. Bigelow, T.M. Koel, J. A. Shaw, Airborne lidar detection and mapping of invasive lake trout in Yellowstone Lake, Appl. Opt. 57 (2018) 4111–4116.
[3] G. Yang, L. Miao, X. Zhang, C. Sun, Y. Qiao, High-accuracy measurement of the focal length and distortion of optical systems based on interferometry, Appl. Opt. 57 (2018) 5217–5223.
[4] Q. Vo, Y. Duan, X. Zhang, F. Fang, Non-contact method of thickness measurement for a transpnt plate using a laser auto-focus scanning probe, Appl. Opt. 58 (2019) 9524–9531.
[5] T. Tao, Q. Chen, J. Da, S. Feng, Y. Hu, C. Zuo, Real-time 3-D shape measurement with composite phase-shifting fringes and multi-view system, Opt. Exp. 24 (18) (2016) 20253, https://doi.org/10.1364/OE.24.02025310.1364/OE.24.020253.v00410.1364/OE.24.020253.v00110.1364/OE.24.020253.v00210.1364/OE.24.020253.v003.
[6] X. Liang, P. Litkey, J. Hyyppä, H. Kaartinen, M. Vastaranta, M. Holopainen, Automatic stem mapping using single-scan terrestrial laser scanning, IEEE Trans. Geosci. Remote Sens. 50 (2012) 661–670.
[7] H. Wang, B. Wang, B. Liu, X. Meng, G. Yang, Pedestrian recognition and tracking using 3D LiDAR for autonomous vehicle, Robot. Auton. Syst 88 (2017) 71–78.
[8] P. Du, F. Zhang, Z. Li, Q. Liu, M. Gong, X. Fu, Single-photon detection approach for autonomous vehicles sensing, IEEE Trans. Veh. Technol 69 (2020) 6067–6078.
[9] L. Wang, Y. Zhang, J. Wang, Map-based localization method for autonomous vehicles using 3D-LIDAR, IFAC-PapersOnLine 50 (2017) 276–281.
[10] Y. Altmann, S. Mclaughlin, M.E. Davies, Fast online 3D reconstruction of dynamic scenes from individual single-photon detection events, IEEE Trans. Image Process 29 (2020) 2666–2675.
[11] B. Du, C. Pang, D. Wu, Z. Li, H. Peng, Y. Tao, E. Wu, G. Wu, High-speed photon-counting laser ranging for broad range of distances, Sci Rep 26 (2018) 1–6.
[12] A. McCarthy, R.J. Colins, N.J. Krichel, V. Fernández, A.M. Wallace, G.S. Buller, Long-range time-of-flight scanning sensor based on high-speed time-correlated single-photon counting, Appl. Optics 48 (2009) 6241–6251.
[13] S. Chen, D. Liu, W. Zhang, L. You, Y. He, W. Zhang, X. Yang, G. Wu, M. Ren, H. Zeng, Z. Wang, X. Xie, M. Jiang, Time-of-flight laser ranging and imaging at 1550 nm using low-jitter superconducting nanowire single-photon detection system, Appl. Opt. 52 (2013) 3241–3245.
[14] A. Perri, J.H. Gaida, A. Farina, F. Preda, D. Viola, M. Ballottari, J. Hauer, S. De Silvestri, C. D'Andrea, G. Cerullo, D. Polli, Time- and frequency-resolved fluorescence with a single TCSPC detector via a Fourier-transform approach, Opt. Exp. 26 (3) (2018) 2270, https://doi.org/10.1364/OE.26.002270.
[15] Z. Bao, Y. Liang, Z. Wang, Z. Li, E. Wu, G. Wu, H. Zeng, Laser ranging at few-photon level by photon-number-resolving detection, Appl. Opt. 53 (2014) 3908–3912.
[16] A. McCarthy, N.J. Krichel, N.R. Gemmell, X. Ren, M.G. Tanner, S.N. Dorenbos, V. Zwiller, R.H. Hadfield, G.S. Buller, Kilometer-range, high resolution depth imaging via 1560 nm wavelength single-photon detection, Opt. Exp. 21 (7) (2013) 8904, https://doi.org/10.1364/OE.21.00890410.1364/OE.21.008904.m001.
[17] R. Brown, P. Hartzell, C. Glennie, Evaluation of SPL100 Single Photon Lidar Data, Remote Sens 12 (4) (2020) 722.
[18] Z. Li, E. Wu, C. Pang, B. Du, Y. Tao, H. Peng, H. Zeng, G. Wu, Multi-beam single-photon-counting three-dimensional imaging lidar, Opt. Exp. 25 (9) (2017) 10189, https://doi.org/10.1364/OE.25.010189.
[19] T. Zheng, G. Shen, Z. Li, L. Yang, H. Zhang, E. Wu, G. Wu, Frequency-multiplexing photon-counting multi-beam LiDAR, Photon. Res 7 (2019) 1381–1385.
[20] X. Ren, Y. Altmann, R. Tobin, A. Mccarthy, S. Mclaughlin, G.S. Buller, Wavelength-time coding for multispectral 3D imaging using single-photon LiDAR, Opt. Express 26 (23) (2018) 30146, https://doi.org/10.1364/OE.26.030146.
[21] Y. Jiang, S. Karpf, B. Jalali, Time-stretch LiDAR as a spectrally scanned time-of-flight ranging camera, Nat. Photonics 14 (1) (2020) 14–18.
[22] Y. Liang, E. Wu, X. Chen, M. Ren, Y. Jian, G. Wu, H. Zeng, Low-timing-jitter single-photon detection using 1-GHz sinusoidally gated InGaAs/InP avalanche photodiode, IEEE Photon. Technol. Lett. 23 (2011) 887–889.
[23] M. Ren, X. Gu, Y. Liang, W. Kong, E. Wu, G. Wu, H. Zeng, Laser ranging at 1550 nm with 1-GHz sine-wave gated InGaAs/InP APD single-photon detector, Opt. Express 19 (14) (2011) 13497, https://doi.org/10.1364/OE.19.013497.
[24] J.M. Rüeger, Refractive indices of light, infrared and radio waves in the atmosphere, School of Surveying and Spatial Information Systems,, University of New South Wales, Sydney, Australia, 2002.